Understanding the Effects of Doping a Regular E10 Gasoline with EHN in an HCCI Engine: Experimental and Numerical Study

Seokwon Cho and Dario Lopez Pintor*

Sandia National Laboratories, 7011 East Ave, Livermore, CA 94550, USA

Abstract

In this study, the effects of doping a regular E10 gasoline with 2-ethlyhexyl nitrate (EHN) are investigated under homogeneous charge compression ignition conditions. Experiments are performed in a 1-liter single-cylinder engine fueled with both straight and EHN-doped E10 gasoline. Numerical studies are performed with an internal combustion engine single-zone reactor utilizing detailed chemical kinetic mechanism with EHN and NO_x chemistry and a surrogate fuel. The kinetic model reproduces the experimental data well for the straight fuel at high initial temperature (T_{BDC}) conditions, whereas the low temperature heat release (LTHR) is under-predicted. Adding EHN reduces the required T_{BDC}, while EHN thermal decomposition rate has to be significantly reduced to accurately reproduce the experimental result, by preventing over-estimation of EHN effect and LTHR. EHN decomposition generates NO_2 and 3-heptyl radicals. Using the well-matched mechanism, the numerical results indicate that among the product of EHN decomposition, NO_2 decreases the autoignition reactivity whereas the production of 3-heptyl radical is the main source for enhancing the low-to-intermediate chemistry by which OH production is accelerated. The production of 3-heptyl radical is highly sensitive to the EHN decomposition reactions. Despite the reactivity enhancement, increase in NO_x emission is observed when the fuel-doping increases.

Keywords: EHN; HCCI; Autoignition Reactivity; NOx Emissions

* Corresponding Author: Dario Lopez Pintor, dlopezp@sandia.gov

Introduction

Homogeneous charge compression ignition (HCCI), as well as other low temperature combustion (LTC) strategies, can be implemented in an engine providing high thermal efficiencies and ultra-low emissions of NO_X and particulate matter [1], [2]. Despite these advantages, there are several technical challenges to overcome before realization of a production HCCI engine. These include: 1) controlling the combustion phasing, 2) obtaining high thermal and combustion efficiencies at low loads, 3) extending the operating map to high loads, and 4) appropriate fuel selection and specification [1]. Research and development has led to substantial progress in understanding the fundamentals and how various strategies can be employed to address these challenges, but further work remains. In particular, the effects of fuel properties on the combustion performance and emissions of HCCI engines have been widely studied with researchers continuing to investigate which fuel properties best enable LTC.

Among all, gasoline is considered a suitable fuel for HCCI combustion due to its high volatility and easy vaporization, which enhances the mixture formation [3]. However, at naturally aspirated conditions and typical compression ratios, the compression heating from the piston motion is not sufficient to ignite the charge without heating the intake air or retaining hot residuals. This challenge can be overcome by enhancing the gasoline reactivity by highly boosting the intake pressure (P_{in} > 200 kPa) [1], [4]–[8]. At these conditions, gasoline exhibits a two-stage ignition pattern, leading to a smoother HRR and improved combustion stability, allowing for higher loads without knocking [6]–[8]. However, substantial amounts of hot residuals or high intake temperatures (T_{in}) are still required for low-to-medium intake pressures. This leads to lower charge densities than those found in conventional engines, limiting the maximum engine load at a given intake pressure. Moreover, intake air heaters or valve timing strategies to supply sufficient heat add complexity and cost to the engine, which may act as a barrier to production. Although

these problems can be substantially reduced using a low-octane gasoline, as discussed by Dec et al. [9], such a gasoline is not readily available in the market.

An alternative to using a low octane gasoline is to dope the fuel with an additive that increases the autoignition reactivity. One well-known additive is 2-ethylhexyl nitrate (EHN), often used to increase the cetane number of diesel fuel [10]–[12] and that has been extensively used to improve diesel engine performance [13]–[17]. Several researchers have shown that EHN has a similar reactivity enhancement effect to fuels in HCCI-like engines [9], [10], [18], [19]. Reitz and co-workers [20]–[22] found that EHN can enhance the reactivity of high octane number fuels such as gasoline, E10, ethanol, and methanol. Hosseini et al. [23] showed that small amount of EHN can advance the LTHR when a doped low-cetane fuel derived from oil sands was tested in a single-cylinder Cooperative Fuel Research engine. Ji et al. [24] also found that the autoignition reactivity of regular-grade E10 gasoline could be enhanced by adding EHN under HCCI-like conditions. At naturally aspirated conditions, the enhanced reactivity allowed significantly reduced intake temperature requirements while only using a very small additive concentration (<0.4%vol). This resulted in a much higher charge density and gross indicated mean effective pressure ($IMEP_g$) compared to the straight fuel. They also found that the EHN doped gasoline underwent two-stage ignition at P_{in} = 100 kPa, whereas straight gasoline typically does not exhibit this behavior at this intake pressure. Even at a slightly boosted condition (P_{in} = 130 kPa), the EHN doping amplified the two-stage ignition process. This improved the combustion stability allowing a more retarded combustion phasing (CA50), contributing to a substantially increased high load limit (30% increase at P_{in} = 100 kPa and 22% increase at P_{in} = 130 kPa). NO_x emissions increased proportionally to the concentration of the additive, with approximately 30% of the EHN nitrate group converted to NO_x, consistent with the values reported by Dempsey [22] and Ickes [25].

Although EHN is commonly used as a cetane number improver, only a few investigations have been performed to understand the fundamentals of how EHN affects the autoignition chemistry.

Tanaka et al. [26] used a rapid compression machine (RCM) to study the effect of EHN on the autoignition characteristics of several pure hydrocarbon species, of which the ignition were reduced when the fuels were doped. Goldsborough et al. [27] also used an RCM to perform an experimental and modeling study of two gasoline surrogates added with EHN. The simulations used a detailed chemical kinetic mechanism that included EHN and NO_x sub-models, however the EHN chemistry in the models overestimated the reactivity enhancement compared to the experiments. Hartmann et al. [28] studied the ignition delay times, flame structure, and intermediate species of EHN-doped n-heptane/air mixtures in a shock tube and in a low-pressure burner. Simulations were performed to replicate the shock tube experiments using an n-heptane mechanism that was manually modified to include EHN chemistry. The authors found that formation of heptyl radicals during EHN's thermal decomposition was the main source of the ignition enhancement of doped fuel. Almodovar and Goldsmith [29] also found an important chemical activity related to the 3-heptyl radical by measuring the decomposition kinetics of EHN in a shock tube in a recent study. Finally, Stein et al. [30] investigated the chemical effects of EHN on the autoignition behavior of surrogate diesel fuel mixtures in a flow reactor, proposing a phenomenological mechanism for EHN decomposition. As described, chemical kinetic studies on EHN were performed in RCMs, shock tubes or flow reactors, but investigations under HCCI-like engine conditions has not been reported yet in the literature.

To understand how EHN enhances autoignition chemistry, several authors have proposed simple mechanisms to describe the chemical pathways that occur during the decomposition of EHN into formaldehyde (CH_2O), NO_2, and 3-heptyl (C_7H_{15}-3) radicals, and other minor species. Among these, CH_2O does not seem to cause the ignition enhancement, since high CH_2O concentrations (~1000 ppm) are required to have a noticeable effect on the ignition delay [29]. NO and NO_2 generated from EHN has generally been considered as the main species to enhance the reactivity; previous work has shown that even a few ppm of NO_x can advance the combustion

phasing under engine conditions [4], [31], [32]. However, recent studies [27], [28] suggest that the 3-heptyl radical plays the key role in improving the ignition quality instead of NO_x. Therefore, to better understand the actual mechanism of how EHN increases the autoignition reactivity, the role of NO_2 and the 3-heptyl radical in the ignition process needs to be further investigated, particularly under HCCI operating conditions.

In this study, effect of EHN doping to a full boiling range E10 gasoline is investigated in an HCCI engine. The main advantage of using an HCCI engine is that the evaluation of EHN-doped fuel is enabled under transient pressure-temperature (P-T) conditions. Residence time at each P-T during the compression stroke plays a significant role as the time available for the chemistry affect EHN's impact on base fuel's reactivity, so studies only using RCMs or shock tubes have some limitations.

In the next section, the experimental setup is described in detail including the engine facility, data acquisition and analysis techniques, fuel/additive properties, and test conditions. This is followed by a description of the numerical approach, in which a gasoline surrogate fuel is proposed along with a detailed kinetic mechanism that contains EHN and NOx sub-models. Results are then presented in three sub-sections: 1) validation of the kinetic model, 2) experimental and numerical results showing the EHN reactivity enhancement, and 3) experimental and numerical analyses of NOx emissions. Finally, the main conclusions from this study are stated.

Experimental Setup

Engine Facility

A single-cylinder engine modified for low-temperature gasoline combustion (LTGC) research was used in this investigation. This engine is derived from a Cummins B-series, six-cylinder, diesel engine, which is a typical medium-duty diesel engine with a displacement of 0.98 liters/cylinder, and had been converted for single-cylinder operation by deactivating cylinders 1-5, as shown in Fig. 1(a). Combustion analysis and modeling require low level of uncertainty when chemistry and

ignition process studies are involved. Using multi-cylinder engine has an advantage of being close to practical when evaluating engine performance, however, the sources of the uncertainties can be spread and not limited to: different trapped mass per cylinder, boundary and initial conditions affected by cylinder-to-cylinder interactions. In addition, facility requirement for lowering uncertainty can be unrealistic. Therefore, it was decided to use a single-cylinder engine in this study.

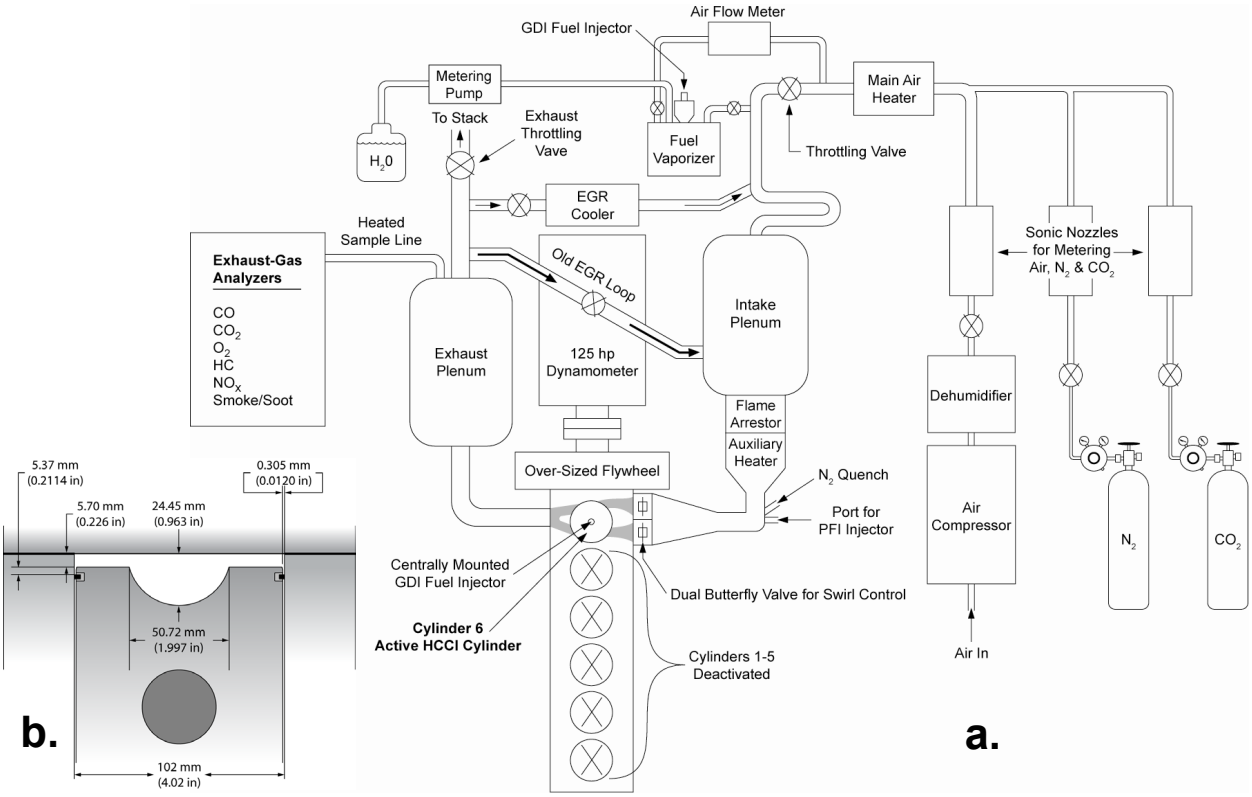

Figure 1. (a) Schematic of HCCI engine facility; (b) Combustion chamber geometry at top dead center (TDC) with the CR = 14:1 piston

The compression ratio (CR) of the active cylinder can be modified by using custom pistons; a piston providing a CR = 14:1 was chosen for this study. This piston was designed to have an open combustion chamber with a quasi-hemispherical bowl and a large squish clearance, as shown in Fig .1(b). The main engine specifications are listed in Table 1. Further details about the engine facility configuration can be found in previous studies performed with gasoline [33]–[35] and low-octane fuels [8], [36], [37] in the same facility. A premixed fueling system, which is shown at the

top of Fig. 1(a), was used to thoroughly mix the fuel and air prior to intake. A gasoline direct injection (GDI) fuel injector assembled to an electrically heated fuel-vaporizing chamber, and appropriate plumbing was used to ensure thorough premixing with the air. A positive displacement fuel flow meter (Max P002), with a reported accuracy of ±0.2%, was used to determine the amount of fuel supplied to the engine.

Table 1. Engine specification and operating condition

Displacement (per cylinder)	0.981 liters
Bore	102 mm
Stroke	120 mm
Connecting rod length	192 mm
Geometric compression ratio	14:1
Number of valves	4
IVO	0° CA aTDC[1]
IVC	202° CA aTDC
EVO	482° CA aTDC
EVC	8° CA aTDC
Swirl ratio	0.9
Fueling system	Fully premixed, GDI
Engine speed	1200 rpm
Intake pressure (abs.)	100 ~ 180 kPa
Intake temperature	60 ~ 145°C
Coolant/oil temperature	100°C

Intake air was supplied by an air compressor and the moisture was removed using a dehumidifier. The airflow was precisely metered by a sonic nozzle with an uncertainty of ±0.25%. N_2 and CO_2 were also introduced using sonic nozzles to provide synthetic EGR instead of reintroducing actual exhaust gases because species such as NOx, water, or partially oxidized hydrocarbons can affect the autoignition chemistry. The N_2/CO_2 blend ratio was adjusted to have the same specific heat capacity (C_p) as the complete stoichiometric products so that the thermodynamic effect of water was taken into account despite its absence.

[1] 0° CA is defined as TDC intake. The valve-event timings correspond to 0.1 mm lift.

An equivalence ratio based on the total charge-mass (ϕ_m) is used as the follows:

$$\phi_m = \frac{(F/C)}{(F/A)_{stoich}} \quad \text{Eq. 1}$$

where (F/C) is the mass ratio between fuel and charge gas (i.e., air plus EGR), and $(F/A)_{stoich}$ is the stoichiometric fuel/air mass ratio for complete combustion. This provides a convenient and consistent way to compare data with the same supplied energy content per unit charge mass (i.e., the same dilution level) for operating conditions with different fuels and different EGR levels. It should be noted that ϕ_m coincides with the conventional air-based ϕ when no EGR is used. Moreover, the air-based ϕ_m is less than unity for all the operating points presented, so that no rich condition was achieved during the experiment. The overall uncertainty in ϕ_m is calculated as ±0.32% based on the errors in air and fuel flow rate measurements.

The intake pressure varied from 100 kPa to 180 kPa. Electrical heaters were installed on the cooling water and lubricating-oil circulation systems, the temperatures were set to 100°C for all testing conditions. In addition, the intake tank and plumbing were preheated to 50°C to avoid fuel condensation. An auxiliary heater mounted close to the engine provided precise control on the intake temperature, which could be controlled from 60°C to 310°C. All temperatures were measured with K-type thermocouples with an uncertainty of ±0.5°C. Finally, all data were taken at an engine speed equal to 1200 rpm.

Data Acquisition

In-cylinder pressure was measured using a piezoelectric transducer AVL QC33C mounted in the cylinder head approximately 42 mm off-center. The pressure signal was digitized and recorded at 0.25° crank angle (CA) increments for one hundred consecutive cycles. Zero-level correction for in-cylinder pressure was carried out by referencing to the intake pressure near bottom dead center (BDC) where the cylinder pressure was virtually constant for several degrees. Intake pressure was measured using a Taber M2911 bonded strain gage transducer, and exhaust pressures were

177 measured using a Kistler 4075A piezo-resistive sensor coupled to a Kistler 7531 cooled switching
178 adapter. BDC temperature before the compression stroke (T_{BDC}) was evaluated with procedure
179 described in [34] for each operating point. Finally, 0°CA is defined as TDC intake in this study, so
180 that TDC compression is at 360°CA. This way, negative crank angles or notations using before
181 top dead center (bTDC) or after top dead center (aTDC) are avoided for clarity.

182 The CA of 50% burn point (CA50) was used to monitor the combustion phasing, whereas the CA
183 of 10% burn point (CA10) was used as an indicator of high-temperature autoignition point. CA10
184 and CA50 were determined from the cumulative apparent heat release rate (AHRR), computed
185 from the cylinder pressure data after applying a 2.5 kHz low-pass filter [38]. The start of heat
186 release is set at the minimum point of the AHRR curve before the main heat release peak. For a
187 two-stage ignition case, this minimum point is located between the LTHR peak and main heat
188 release peak. This method provides a consistent measurement to compare the CA10 and CA50
189 of the main combustion event, excluding the effect of LTHR from the burn-duration calculation.
190 Computations of CA10 and CA50 were performed for each individual cycle, disregarding heat
191 transfer and assuming a constant specific heat ratio ($\gamma = C_p/C_v$). The HRR signal was computed
192 from the 100-cycle averaged pressure trace (with the 2.5 kHz low-pass filter applied) [39],
193 assuming the Woschni correlation for heat transfer [40] and computing the specific heat ratio for
194 each time step. These results are mainly used to analyze the low-to-intermediate temperature
195 heat release rate that occurs before the high-temperature ignition.

196 Exhaust gas was collected downstream of the exhaust plenum using a heated sample line (see
197 Fig. 1(a)). CO, CO_2, unburned hydrocarbons (HC), nitrogen oxides (NOx), and O_2 were measured
198 using standard exhaust-gas analysis equipment as used in previous studies [35]. Soot emissions
199 were monitored using an AVL smoke meter, and were found to be below the detectability limit for
200 all data reported. The results of exhaust gas measurements is within ±1% uncertainty range.

Ringing intensity (RI) developed by Eng [38] given in equation 2, which has been widely accepted in HCCI studies [41], [42], was used to evaluate the level of knock during the operation:

$$RI \approx \frac{1}{2\gamma} \cdot \frac{\left(0.05 \cdot \left(\frac{dP}{dt}\right)_{max}\right)^2}{P_{max}} \cdot \sqrt{\gamma R T_{max}} \qquad \text{Eq. 2}$$

where $(dP/dt)_{max}$, P_{max}, and T_{max} are the maximum pressure rise rate, pressure, and temperature, respectively, γ is the specific heat ratio, and R is the gas constant. The limit for ringing intensity was set to 5 MW/m^2, which corresponds to approximately 8 bar/°CA at 1200 rpm under naturally aspirated conditions. Anecdotally, this limit showed a very good correspondence with the onset of audible knocking sound and ripple appearance on the pressure trace during the experiment. In addition, noticeable engine knock also correlated well for all boost levels tested, giving confidence to this correlation, whereas 3 MW/m^2 was more pertinent and set as the limit for naturally aspirated conditions. Throughout the current work, data were collected under conditions at which combustion was near non-sooting, complete (combustion efficiency > 95%), stable (coefficient of variation (COV) of IMEPg ≤ 1%), and not knocking, unless otherwise noted.

Fuel and Additive Properties

A regular commercial gasoline containing 10%vol ethanol (E10), hereafter referred as base fuel, is used in the current study. Table 2 lists the main properties of this fuel. EHN with a purity of 97% was used to dope the base fuel (most of the impurity is from isomers). The additive was properly mixed with the base fuel on a volume percentage basis, and the physical properties of the fuel mixtures were calculated based on the fuel specifications.

Table 2. Fuel properties of E10 base fuel

Formula	$C_{5.76}H_{11.98}O_{0.22}$
Specific gravity (15°C)	0.7238
Lower Heating Value, MJ/kg	41.74
Carbon, wt. %	81.67
Hydrogen, wt. %	4.06
RON	92.5

MON	84.6
Anti-knock Index (RON+MON)/2	88.6

Modeling Approach

Kinetic model and engine parameters setup

A detailed gasoline surrogate mechanism was used for kinetic model in the present work, and the mechanism has been modified to include EHN and NO/NO_2 sub-mechanisms. The original mechanism was provided by Lawrence Livermore National Laboratory (LLNL) [43], and includes low-temperature and high-temperature chemistry of four hydrocarbon species: n-heptane, iso-octane, 2-pentene, and toluene. An ethanol sub-mechanism is also included. This modified mechanism has been used to replicate HCCI experimental data at high boosted conditions, where conventional gasoline was used without ethanol [44]. The EHN sub-mechanism was adopted from [45] and [36], which contains the following two reactions:

$$EHN \Leftrightarrow EHO + NO_2 \qquad R1$$

$$EHO \Leftrightarrow CH_2O + C_7H_{15}\text{-}3 \qquad R2$$

R1 describes initial decomposition of EHN into NO_2 plus ethylhexyloxy (EHO) radical. Since EHO is considered to be an unstable species, it rapidly decomposes through scission reactions shown in R2. The NO/NO_2 sub-mechanism used was initially developed by Rasmussen et al. for low-to-intermediate temperatures [46], which are similar to the conditions in this study. The combined kinetic mechanism consists of 1404 species and 6025 reactions.

Simulations of the experiments were carried out using the CHEMKIN-PRO single-zone internal combustion engine reactor. The initial crank angle for the simulations was set at 180°CA (BDC), and computations were performed until 260°CA (about halfway through the compression stroke). The BDC pressure in the simulations was specified to match the experimental data. An effective compression ratio of 13:1 was also imposed on the simulations; a similar approach has been successfully used by others including Sjöberg and Dec [1], [47] and validated by comparison with multi-zone simulations.

Since the chemical kinetics that governs the ignition are sensitive to evolution of the in-cylinder temperature during cycle, it is important to accurately model the wall temperature and heat transfer to match the experimental conditions. The experimental fire-deck temperature for each condition was used as wall temperature of the simulation. To signify the role of heat transfer on the simulation error, pressure and temperature profiles obtained under motoring conditions at P_{in} = 100 kPa and T_{in} = 151°C are plotted in Fig. 2. Three different results are plotted: 1) experimental data, 2) an adiabatic simulation, and 3) a simulation considering heat losses. In the case that the heat transfer in incorporated (dashed line), the same Woschni correlation [40] and coefficients used to account for the heat losses in the experiment, was applied to the simulation. It can be seen that the case closely matches the experimental pressure and temperature profiles as well as combustion phasing, peak pressure and temperature, whereas the adiabatic simulation fails to reproduce. For this reason, the heat loss correction is applied to all conditions discussed on the following sections.

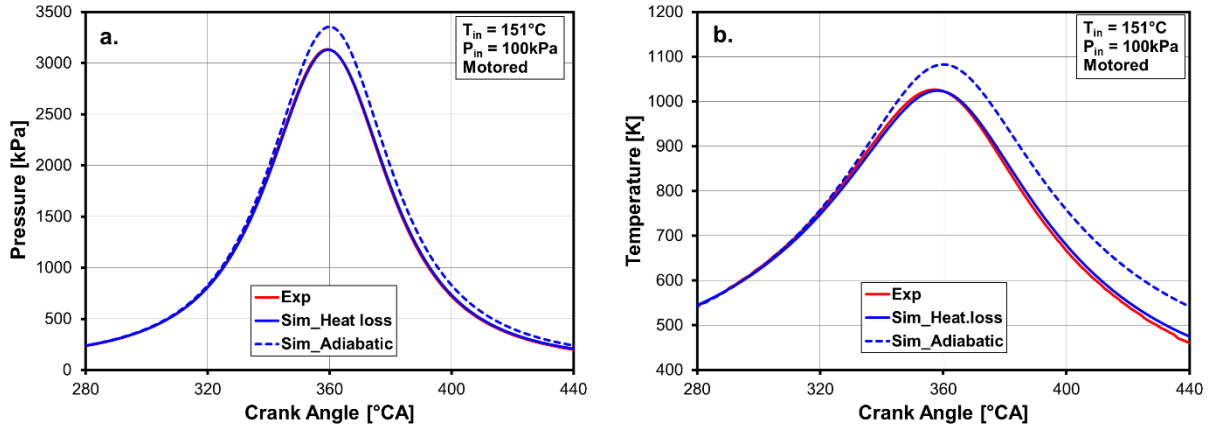

Figure 2. Comparison between conditions with heat loss and without heat loss (adiabatic) in a single zone model simulation under motoring conditions at P_{in} = 100 kPa and T_{in} = 151°C

Fuel Surrogate

The chemical composition of a real base gasoline has too much complexity for modeling, so a simple mixture, a surrogate fuel that reproduces the main ignition characteristics of the base fuel, is used instead. A five-components surrogate mixture for E10 gasoline is proposed in this work,

264 which includes the main hydrocarbon classes present in the base fuel: n-alkanes (n-heptane),
265 iso-alkanes (iso-octane), olefins (2-pentene), aromatics (toluene), and oxygenates (ethanol). The
266 surrogate formulation was designed to match the molar composition of each hydrocarbon class
267 in the base fuel as closely as possible. However, the base fuel contains some cyclo-alkanes,
268 which are missing from the chemical kinetic mechanism. For this reason, all cyclo-alkanes were
269 substituted by n-heptane in the surrogate fuel. The final composition can be seen in Table 3. It is
270 noteworthy that H/C ratio and lower heating value (LHV) are similar to those of the base fuel.

271 Table 3. Gasoline and surrogate specifications

	Base fuel	Surrogate fuel	
N-alkanes, mol	0.15	0.21	(n-heptane)
Iso-alkanes, mol	0.38	0.38	(iso-octane)
Olefins, mol	0.03	0.03	(2-pentene)
Cyclo-alkanes, mol	0.06	0	(not available in mechanism)
Aromatics, mol	0.17	0.17	(toluene)
Oxygenates, mol	0.21	0.21	(ethanol)
H/C	2.082	2.093	
LHV, J/g	41677	42182	

272 For performance verification of the surrogate fuel in simulation referenced to base fuel in the
273 experiment, the relationship between T_{BDC} and the combustion phasing at P_{in} = 100 kPa and ϕ =
274 0.4 is plotted in Fig. 3 (a). As expected, a higher T_{BDC} advances the combustion timing for all
275 results. The simulation shows slightly more retarded combustion phasings (CA10 and CA50) are
276 slightly more retarded for the simulations for 2-4°CA, but the experimental trends are properly
277 captured, and both CA10 and CA50 slopes are replicated with high accuracy. Fig. 3 (b) shows
278 the LTHR and intermediate-temperature heat release (ITHR) for CA10 = 368.4°CA for both the
279 experiment and simulation. 4.5 K higher T_{BDC} was required in the simulation to match the
280 experimental combustion timing. Although the combustion phasing indicators show slight
281 discrepancies, the early stage of the heat release of experiment is closely reproduced in the
282 simulation.

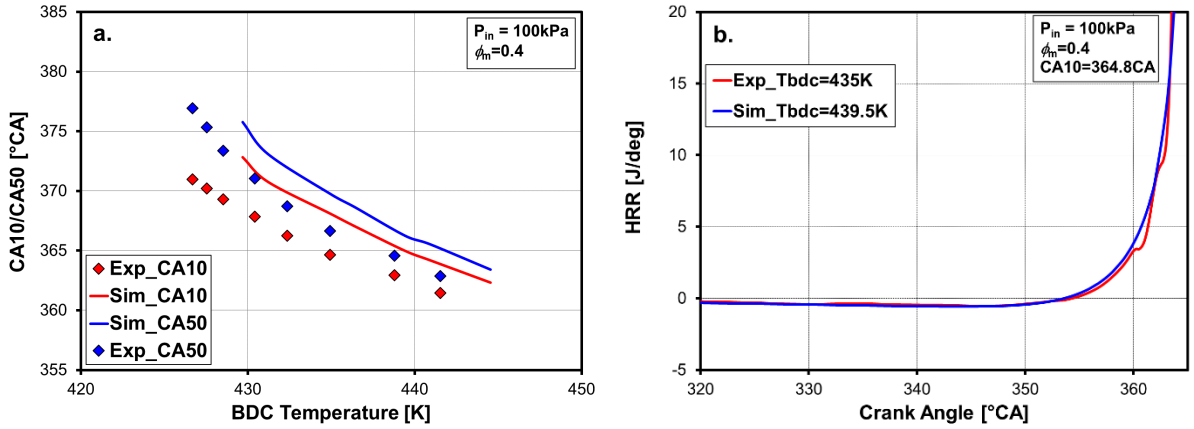

Figure 3. Comparison between the base fuel (experiment) and the surrogate fuel (simulation) at P_{in} = 100 kPa and ϕ_m = 0.4: (a) T_{BDC} and combustion phasing; (b) HRR profiles for a matching CA10 = 364.8°CA.

Although the suggested surrogate fuel shows a good performance in replicating the heat release and is not complex, developing more developed one with other higher carbon component would be viable to evaluate the effect of EHN, with some extent of sensitivity analyses.

Results and Discussion

Base Fuel

The simulation is compared to experiment when the fuels (the base fuel and surrogate) are straight, without EHN. In Fig. 4, the required T_{BDC} to reach the knock limit at several intake pressures and two different EGR concentrations of 21.7% and 47.2% are shown.

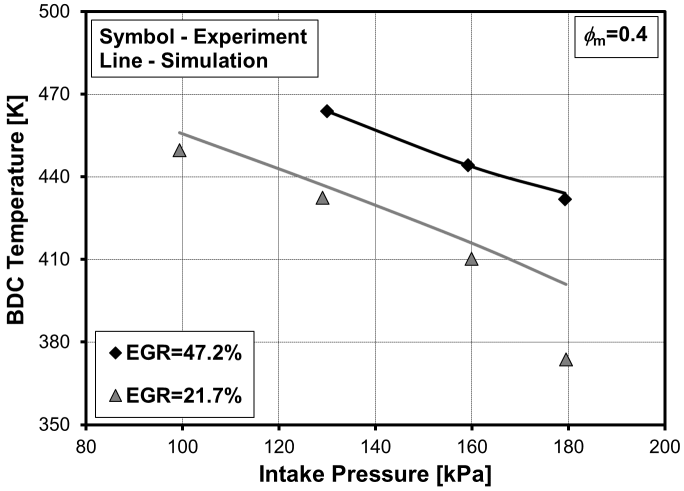

Figure 4. T_{BDC} vs. P_{in} for a ϕ_m = 0.4 base fuel at EGR = 47.2% and 21.7%. RI = 3 MW/m² for P_{in} = 100 kPa and RI = 5 MW/m² for higher intake pressures.

T_{BDC} is adjusted in the simulations to match the experimental CA10 values that are reported in Table 4. The experimental results are given by the data markers, while the results of the simulation are given by a solid line. As shown in Fig. 4, T_{BDC} is reduced as P_{in} increases since the fuel/air mixture becomes more reactive with increasing pressure. For higher EGR (47.2%), experimental data at P_{in} = 100 kPa is unavailable because the required T_{BDC} exceeds the limit of the heating system. It can be seen that for higher EGR, the kinetic model perfectly matches the experiment. For lower EGR (21.7%), the kinetic model still has a reasonable agreement with the experimental trends up to P_{in} = 160 kPa, exhibiting a small offset in T_{BDC}. However, the simulation fails to capture the rapid decrease in T_{BDC} of experiment from 160 kPa to 180 kPa and overestimates by 27 K at 180 kPa condition. The appearance of LTHR causes this drastic decrease in T_{BDC}, which is not properly replicated in the simulations (as explained in detail below).

Table 4. Experimental CA10 values used to match BDC temperature (T_{BDC}) in the simulations

	P_{in} = 100 kPa	P_{in} = 130 kPa	P_{in} = 160 kPa	P_{in} = 180 kPa
EGR = 47.2%	-	362.8°CA	365.3°CA	366.9°CA
EGR = 21.7%	364.1°CA	365.5°CA	368.7°CA	371.5°CA

Figure 5 displays the HRR profiles before the high-temperature ignition at P_{in} = 100 kPa (a) and P_{in} = 180 kPa (b), respectively, for a fuel/air mixture with 21.7% EGR. At naturally aspirated conditions (P_{in} = 100 kPa), LTHR is not noticeable and the simulation accurately predicts the HRR. However, when LTHR begins to become prominent, as seen in Fig. 5(b), the simulation no longer matches the experimental result. It is believed that this uncaptured behavior is the reason why T_{BDC} has to be increased by 27 K for matching CA10; because LTHR promotes autoignition [9], [48], [49] leading to lower T_{BDC} values. The entire cycle-alkane class of the surrogate fuel is n-heptane, which is a very reactive species that is prone to exhibit LTHR. So the less reactivity of

the surrogate fuel in the model compared to base fuel is unexpected. Further investigation is necessary to improve the kinetic model, especially under this condition.

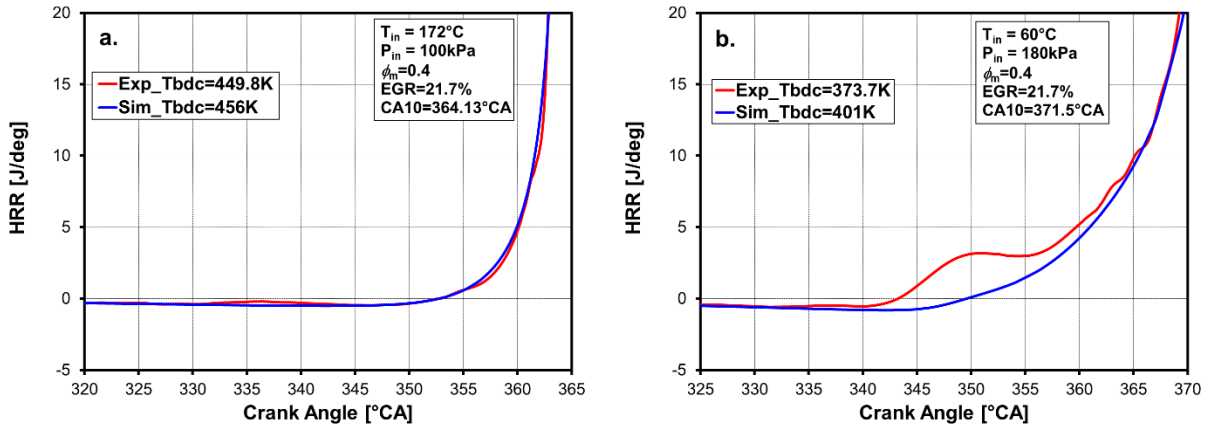

Figure 5. HRR comparison between experiment and simulation for the base fuel with ϕ_m = 0.4 and EGR = 21.7% at (a) P_{in} = 100 kPa and (b) P_{in} = 180 kPa.

Doped Fuel

Experimental T_{BDC} data are presented in Fig. 6(a) at EGR = 47.2% for several intake pressures. Three EHN doping levels are presented: straight base fuel, 0.25% and 0.4% EHN by volume. All data were collected at ϕ_m = 0.4 and CA10 = 366.9°CA. The fuel doped with 0.4% EHN was not tested at P_{in} = 180 kPa because the required T_{in} to prevent knocking was lower than 60°C, close to the point at which fuel begins to condense in the fueling system. Fig. 6(a) shows that the required T_{BDC} is drastically reduced when EHN is added to the base fuel. For instance, comparing the doped fuel to the base fuel at P_{in} = 130 kPa, T_{BDC} was reduced by 24 K with 0.25% EHN and 38K with 0.4% EHN, respectively. The autoignition enhancement with respect to lower required T_{BDC} becomes stronger as intake pressure increases. For example, with 0.25% EHN, T_{BDC} could be reduced by 46 K and 63 K when P_{in} increased to 160 kPa and 180 kPa, respectively. The EHN effect is highly nonlinear with the EHN concentration; the T_{BDC} reduction is much greater when the EHN concentration is increased from none to 0.25%, compared that of from 0.25% to 0.4%. This result is consistent to the observation reported by Ji et al. [24].

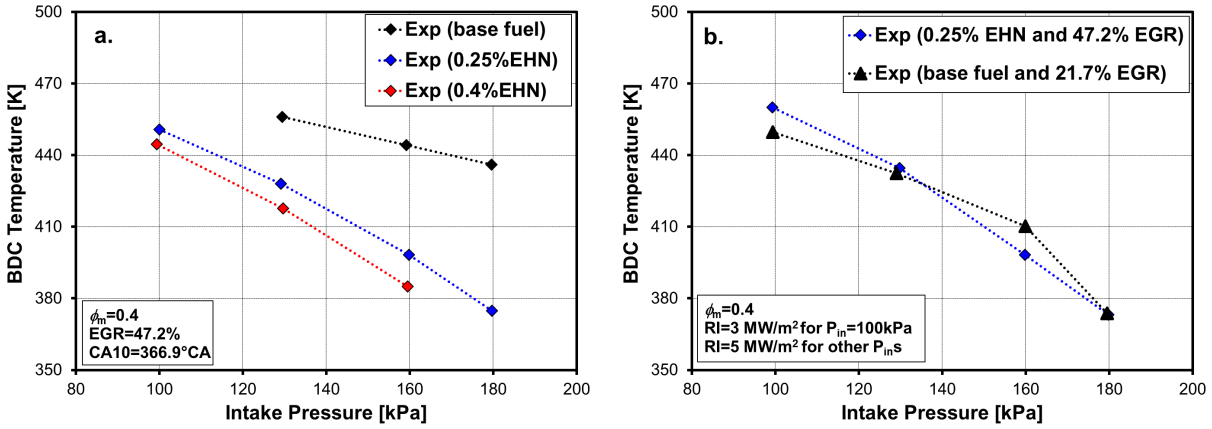

337

338 *Figure 6. Relationships between experimentally determined T_{BDC} and P_{in} with: (a) Base fuel and varying*
339 *EHN levels, CA10 = 366.9°CA and EGR = 47.2%; (b) Maintaining RI = 3 MW/m² at P_{in} = 100 kPa and RI*
340 *= 5 MW/m² for higher intake pressures.*

341 In Fig. 6(a), the T_{BDC} and P_{in} relationships are shown for a fixed EGR level at 47.2% with CA10 =
342 366.9°CA. Fig. 6 (b) shows a different comparison, CA10 varies while the RI is held at the knock
343 limit. It is important to note that the required amount of EGR is reduced to 21.7% to achieve the
344 same RI when the base fuel is used. With the base fuel, a sudden change of slope can be seen
345 between P_{in} = 160 kPa and 180 kPa, which is an indicator of the LTHR onset. There does not
346 appear to be a similar shift in slope with the doped fuel, which suggests that the EHN is changing
347 the low-to-intermediate temperature chemistry.

348 Fig. 7 shows the behaviors of the EHN-doped surrogate fuel (in simulation) and the EHN-doped
349 base fuel (in experiment) for 0.25% and 0.4% EHN by volume. If the EHN level is the same,
350 approximately 37-38 K lower T_{BDC} is required at P_{in} = 100 kPa, and gradually decreases to 16 K
351 lower at P_{in} = 180 kPa. It is apparent that the kinetic model generally over-predicts the autoignition
352 enhancement by EHN, leading to lower required BDC temperatures compared to the experiment.
353 However, if the amount of additive in the simulations is decreased by a factor of 10, the
354 simulations closely match the experiments. This suggests that the chemical kinetics of the additive
355 can be improved by adjusting the rate of specific reaction in the EHN decomposition reactions.

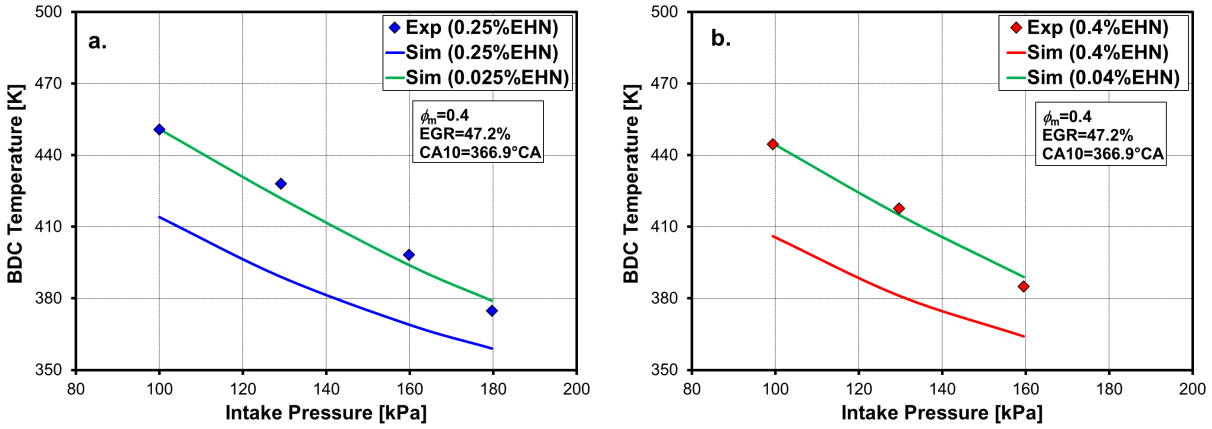

Figure 7. T_{BDC} vs. P_{in} for experiment and simulation at two different doping levels: (a) 0.25% EHN and (b) 0.4% EHN. 10% of each EHN level is also tested in the simulation to closely match the experimental result.

Fig. 8 compares experimental and numerical HRRs at P_{in} = 100 kPa and 160 kPa, which were normalized by the total heat released (THR) to compare different engine loads. Solid lines display the HRR profiles obtained from the experiments with 0.25% EHN, while the simulation results are plotted with dashed (0.25% EHN) and dotted lines (0.025% EHN). The simulation with 0.25% EHN over predicts the LTHR and ITHR, whereas simulations with 0.025% EHN are in good agreement with the experimental data. In fact, the existence or absence of LTHR, as well as its timing and magnitude, are replicated almost perfectly when the EHN concentration is reduced by a factor of 10. This deviation is likely caused by the EHN kinetic model, since the behavior of the straight surrogate fuel tends to under-predict the LTHR (see the discussions referring to Figs. 4 and 5). Thus, the analysis of the HRR further suggests that the chemical kinetics of the additive can be improved by modifying the EHM decomposition reactions.

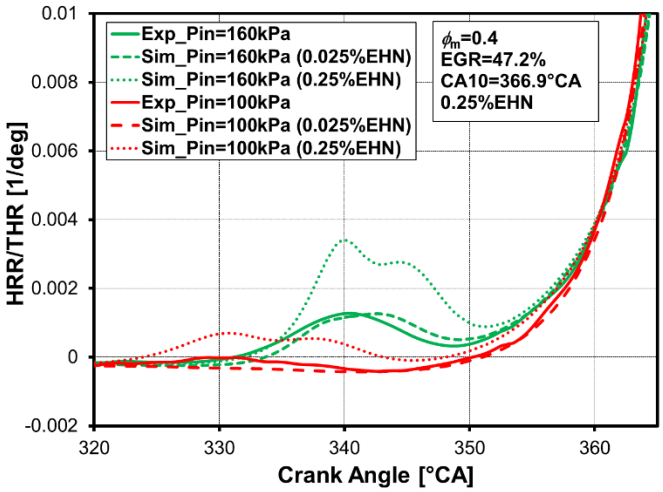

Figure 8. Comparison of normalized HRR profiles for 0.25% EHN

Fig. 9 shows the numerical HRR and the mass-averaged temperature of the surrogate fuel against crank angle for 0.025% EHN at P_{in} = 180 kPa. The 100-times-amplified heat production rate of the EHN decomposition reactions (R1 and R2) is also plotted. LTHR is observed between 335 – 350°CA, and the corresponding temperature varies from 730 K to 880 K. Due to the LTHR, the in-cylinder temperature increases (see the dashed ellipse in Fig. 9), promoting the autoignition of the mixture. Reactions R1 and R2 both occur before the onset of LTHR and are endothermic in nature. However, the HRR and the mass-averaged temperature are not noticeably affected during the phase of R1 and R2, and this suggests that the EHN decomposition has a negligible thermodynamic effect. Therefore, the ignition enhancement must be primarily due to the species evolved and chemical in nature. To better understand which of the species are responsible for the increase in autoignition reactivity, species profiles are plotted in Fig. 10 alongside the HRR and temperature profiles for this simulation. The main species from the EHN decomposition are included (EHO, NO_2, C_7H_{15}-3, and CH_2O), along with NO in order to analyze the NO_2-to-NO conversion ratio.

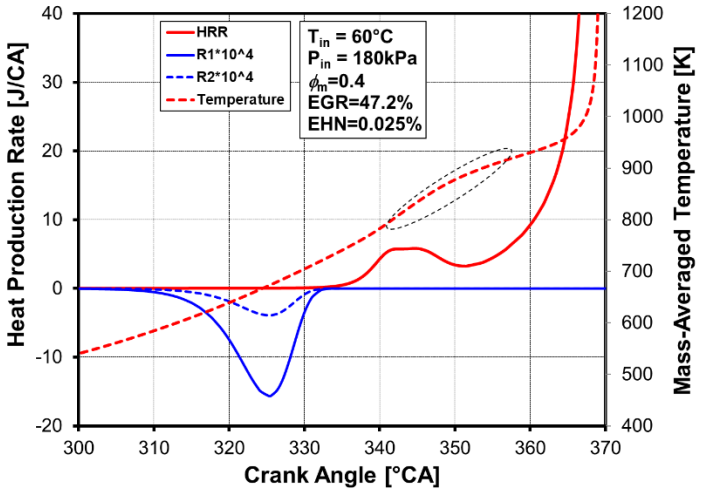

Figure 9. Simulated HRR and temperature profiles for surrogate fuel doped with 0.025% EHN at P_{in} = 180 kPa.

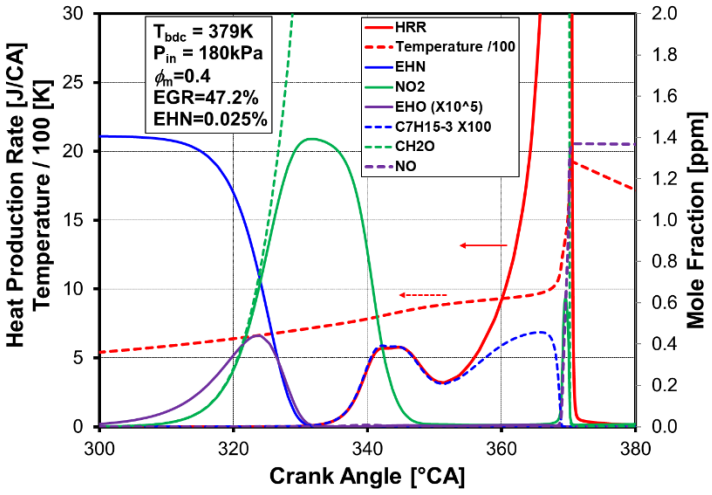

Figure 10. Simulated HRR, temperature, and specie profiles for surrogate fuel doped with 0.025% EHN at = 180 kPa.

EHN is not stable at medium temperatures (above 500 K) and its thermal decomposition described by R1 starts at approximately 310˚CA. The EHO radical is very reactive, therefore the accumulation of EHO is extremely low (5 to 6 orders of magnitude lower than the original EHN concentration). This suggests that EHO rapidly decomposes to C_7H_{15}-3 and CH_2O through reaction R2. Both EHN and EHO are completely consumed before the LTHR starts (near 330˚CA). As expected, CH_2O accumulates during the entire low-to-intermediate temperature regime,

because the CH_2O decomposition to CO is what triggers the high-temperature ignition. In contrast, the NO_2 generated by the EHN decomposition is consumed during the LTHR. However, the NO_2-to-NO conversion is limited, thus NO_2 produces species other than NO during this stage, such as HONO. Only a small amount of NO_2 is found in the high temperature region and it is rapidly reduced to NO, leading to a high NO concentration after the high-temperature stage. The CH_2O generated by EHN does not seem to be the species responsible of enhancing the reactivity. Yamaya et al. [37] proved that hundreds of ppm of CH_2O are needed to have a noticeable effect on the autoignition, while the CH_2O generated by the EHN decomposition is in tens of ppm (one order of magnitude lower than the required amount reported by Yamaya et al.).

To understand the role of NO_2 on the autoignition reactivity, simulations were performed where the initial amount of EHN in the surrogate fuel was substituted by NO_2. The base surrogate fuel was doped with 13.7 ppm of NO_2, which corresponds to a 100% conversion of EHN to NO_2 for the 0.25% EHN-doped base fuel (the amount of EHN used in the experiments). Fig. 11 shows the required T_{BDC} to reach CA10 = 366.9°CA for different intake pressures and fuels. It can be seen that the effect of NO_2 doping decreases the reactivity, requiring approximately 5-6 K higher T_{BDC} to reach the same CA10. Moreover, increasing the initial NO_2 concentration by a factor of 10 further decreases the reactivity. Thus, the NO_2 originating from the EHN decomposition does not seem to be responsible for the faster autoignition. However, previous studies [5], [31], [32] have shown that NO_x (mostly NO) enhance the autoignition reactivity of fuels in HCCI or HCCI-like engines.

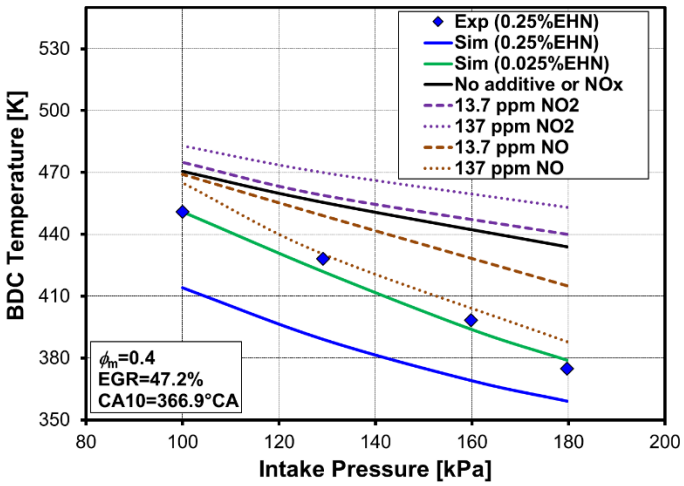

Figure 11. Effect of NO/NO_2 on the autoignition reactivity in simulation.

Effects of NO production by replacing NO_2 was also tested in the simulation, 13.7 ppm of NO assuming 100% conversion of EHN to NO for fuel doped with 0.25% EHN. These results are also presented in Fig. 11 and show that the reactivity is increased, observing a lower T_{BDC} is required to achieve the same CA10. Compared to the base fuel, the required T_{BDC} was reduced by 1 K at P_{in} = 100 kPa and by 19 K at P_{in} = 180 kPa, respectively. However, even though NO acts as an ignition improver, the improvement from a 100% conversion of EHN to NO is not enough to explain the extent of the ignition enhancement by EHN. Although the NO concentration is increased by a factor of 10, the reactivity enhancement (reduction in T_{BDC}) is still less than 0.25% EHN. These results suggest that the NO and NO_2 have very distinct effects on the autoigntion, and should be considered independently when accounting for the effects of NO_x on reactivity.

Referring to Fig. 10 and considering the C_7H_{15}-3 radical, almost no C_7H_{15}-3 is accumulated before the LTHR despite the direct conversion of EHN to C_7H_{15}-3 through reactions R1 and R2. This suggests that C_7H_{15}-3 is very unstable and rapidly consumed. During the LTHR and ITHR, only small amount of C_7H_{15}-3 is accumulated, mainly originating from n-heptane. To elucidate the role of C_7H_{15}-3 playing in enhancing the fuel reactivity, as shown in Fig. 12(a), EHN reaction pathways are constructed from the CHEMKIN results for a simulation with 0.025% EHN-doped fuel at P_{in} =

180 kPa, ϕ_m = 0.40, CA10 = 366.9°CA, and EGR = 47.2%. The timing at which the pathways are constructed is 324°CA, which is the maximum rate of EHN consumption (identified by the inflection point on the EHN concentration in Fig. 10). The width of the arrows qualitatively indicates how much of the original species contributes to the formation of new products.

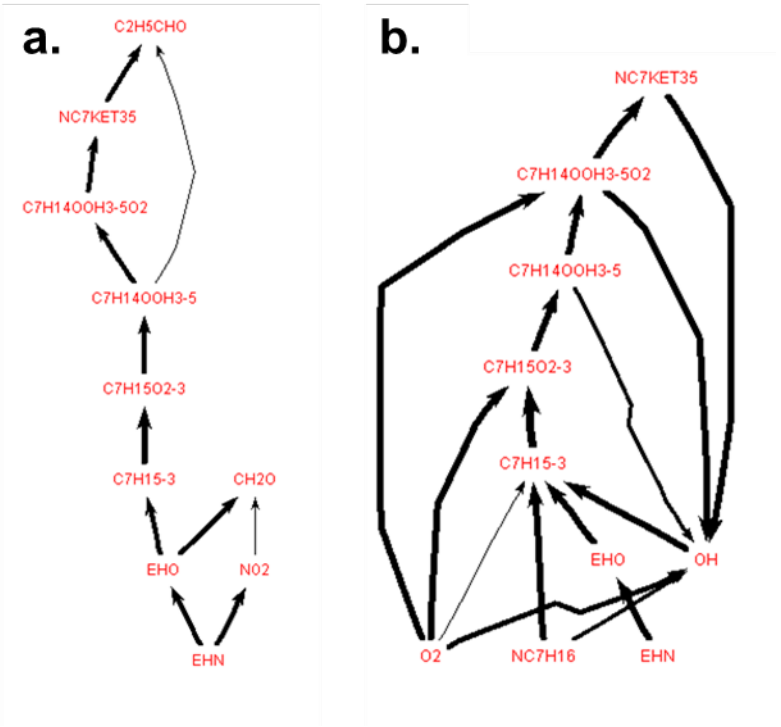

Figure 12. Reaction pathways constructed for the surrogate fuel doped with 0.025% EHN at P_{in} = 180 kPa, ϕ_m = 0.4, CA10 = 366.9°CA and EGR = 47.2%: (a) Decomposition of EHN and (b) OH production from EHN and n-heptane.

As discussed earlier, EHN decomposes into EHO and NO_2 (described by R1), with EHO subsequently reacting to form CH_2O and C_7H_{15}-3 (described by R2). Under these conditions, CH_2O is stable and no further reaction pathway is found for this species. However, the C_7H_{15}-3 continues oxidation by undergoing a typical low-temperature chain-branching reaction. The alkyl radical C_7H_{15}-3 (R•) oxidizes via O2 addition reactions to form C_7H_{15}O2-3 (ROO•) and then C_7H_{14}OOH3-5 (•ROOH) through isomerization. C_7H_{14}OOH3-5 produces OH radicals after a second O2 addition (C_7H_{14}OOH3-5O2), and generates additional OH radicals when this species undergoes isomerization to NC_7KET35. N-heptane contributes to generating both C_7H_{15}-3 and

OH radicals, and a reaction pathway accounting for all OH production at these conditions was constructed and shown in Fig 12.(b). Although n-heptane is also a source of the C_7H_{15}-3 radical, more than 65% of its production during the maximum rate of EHN consumption is attributed to the EHN decomposition. Furthermore, C_7H_{15}-3 was found to be the main source of OH radicals by means of decomposition to C_7H_{14}OOH3-5, C_7H_{14}OOH3-5O2, and NC_7KET35.

As an extension to the reaction pathways, the relative reaction rates are also important for fundamental understanding of EHN's role in autoignition reactivity. It is imperative to note that only the reactions from EHN and n-heptane are included in Figure 12(b), and other species may still be crucial for generating the OH radical pool. Considering all species, Fig.13 shows the OH production/consumption rates for the ten most relevant reactions, evaluated at 324°CA (the timing at which the maximum rate of EHN consumption was achieved). Positive values indicate OH production, whereas negative values indicate OH consumption. It should be mentioned that the net reaction rate (total generation rate minus total consumption rate) governs the formation of the OH radical in the pool. The individual reaction rates that are normalized by the total rate of OH production/consumption, are displayed as percent of the total. Thus, it is seen that the reaction C_7H_{14}OOH35O2 $\Leftrightarrow$ NC_7KET35 + OH represents 24% of the total OH generation rate at this instant. Similarly, the reaction NC_7H_{16} + OH $\Leftrightarrow$ C_7H_{15}-3 + H_2O accounts for 13% of the total OH consumption rate. Most of the OH is generated from the C_7H_{14}OOH3-5O2 and NC_7KET35 radicals (which were generated by the C_7H_{15}-3 radical, as discussed earlier). OH radicals attack the fuel through H-abstraction reactions, generating more alkyl radicals in a chain reaction mechanism. Among all the species that comprise the surrogate fuel, n-heptane is the species most prone to consume OH radicals. This is an expected result because the low-temperature chemistry of long chain n-alkanes is very reactive. However, some of the n-heptane is converted into C_7H_{15}-3, ultimately generating more OH. The chain reaction is accelerated when C_7H_{15}-3 radicals are added to the mixture through EHN thermal decomposition, leading to shorter autoignition time.

For these reasons, the C_7H_{15}-3 radical is considered to be the main species responsible for the autoignition enhancement.

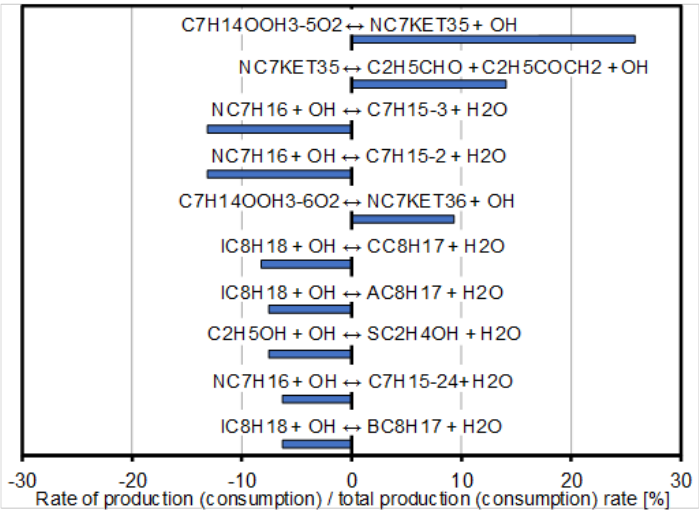

Figure 13. OH relative consumption and production rates at 324°CA for a 0.025% EHN-doped fuel with P_{in} = 180 kPa, ϕ_m = 0.4, CA10 = 366.9°CA and EGR = 47.2%.

A sensitivity analysis was applied to the OH production and consumption reactions at 324°CA (maximum EHN consumption rate), the sensitivity coefficients of which were calculated as follows:

$$S_i = \frac{d(ln(d[OH]/dt))}{d(ln(A_i))} \quad \text{Eq. 3}$$

where $d[OH]/dt$ is the OH net generation rate and A_i is the pre-exponential factor of the specific reaction rate of the i-th reaction. Fig. 14 shows the ten most sensitive reactions, in which a positive value means that the OH production is favored by increasing the reaction rate and vice versa. The main reaction classes to which OH is sensitive are the EHN thermal decomposition (R1), the isomerization of •ROOH radicals and the H-abstraction of the fuel. Results suggest that changing the specific reaction rate of R1 will have a significant impact on the production of OH. Thus, the reactivity overestimation shown by the mechanism in Fig. 7 can be corrected by reducing the pre-exponential factor of R1, leading to a lower OH production and, therefore, to a more realistic prediction of the autoignition enhancement.

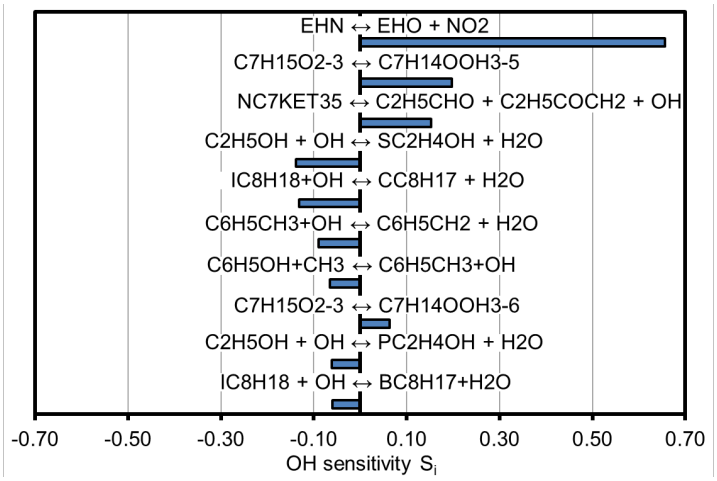

Figure 14. OH sensitivity analysis at 324°CA for a 0.025% EHN doped fuel with P_{in} = 180 kPa, ϕ_m = 0.4, CA10 = 366.9°CA and EGR= 47.2%.

Fig. 15 shows the experimental and numerical T_{BDC} required to obtain CA10 = 366.9°CA For several intake pressures. Figs. 15(a) and (b) display the results for 0.25% and 0.4% EHN-doped fuels, respectively. Two different EHN sub-mechanisms were used. One is the original EHN sub-mechanism adopted from [45] and [36], whose pre-exponential constant of reaction R1 is equal to 10^{16} s^{-1}, and is shown as a solid line. The other one is a modified EHN sub-mechanism, whose pre-exponential constant of R1 is equal to 10^{14} s^{-1} and is indicated with a dashed line. The activation energy of the reaction was kept constant (39 kcal/mol) for both sub-mechanisms. It is shown that the simulations accuracy can be remarkably improved by decreasing the pre-exponential constant for the EHN thermal decomposition by a factor of 100.

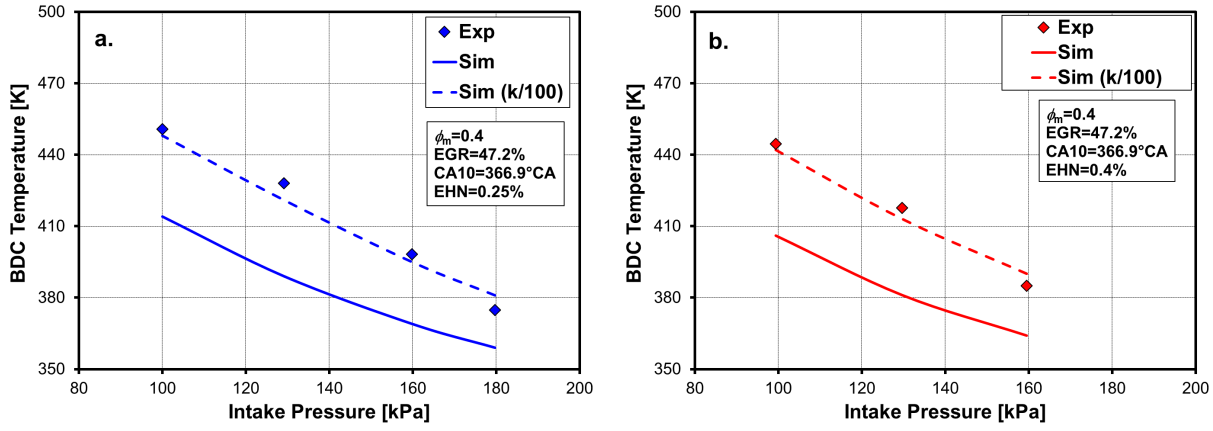

Figure 15. T_{BDC} vs. P_{in} comparison of original and updated EHN sub-mechanism at two different doping levels: (a) 0.25% EHN and (b) 0.4% EHN.

Fig. 16 compares the NO_x emissions from experiment and simulation for the base fuel and two different doping levels, 0.25% EHN and 0.4% EHN. The simulations used the modified EHN sub-mechanism described in the previous paragraph. Despite having lower intake temperatures, the doped fuels have higher NO_x emissions in both the experiment and simulation. More specifically, results with the base fuel show ultra-low NO_x emissions near 1 ppm, whereas they increase up to 3.7–5.1 ppm for 0.25% EHN and up to 7.6–8.7 ppm for 0.4% EHN, respectively.

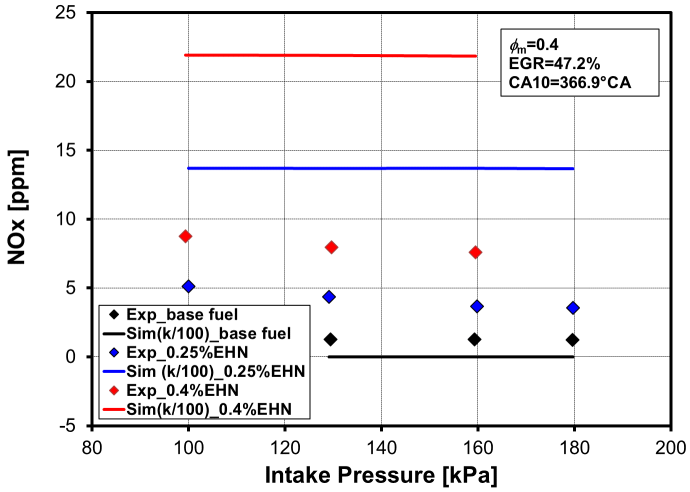

Figure 16. Comparison of NOx emissions between experiments and simulations for the base fuel and two doping levels. Simulations were performed using the updated EHN sub-mechanism.

The measured NO_x emissions is slightly reduced as the intake pressure increases. This might be caused by a reduction in thermal NOx, since the higher the intake pressure, the lower the temperature required to keep the CA10 constant. The kinetic model shows near zero NOx emissions for the base fuel, while it over-predicts the NOx emissions for both doping levels. Moreover, the kinetic model doesn't show any variation in NO_x with increasing P_{in}. The discrepancy in the simulations appears to be mainly from the sub-mechanism inaccurately describing the NO chemistry. The kinetic model shows nearly a 100% conversion of the EHN nitrate group into NO_x, with NO representing nearly 96.5% of NO_x. On the other hand, the

experiments only show a conversion rate between 27-40%, a range similar to those reported by [24].

Fig.17(a) shows the concentration profiles of species that contain nitrogen and for which the maximum concentration is higher than 0.01 ppm in simulation at P_{in} = 180 kPa, ϕ_m = 0.40, EGR = 47.2% and 0.25% EHN doping level, using the modified EHN sub-mechanism (EHN decomposition rate reduced by a factor of 100).

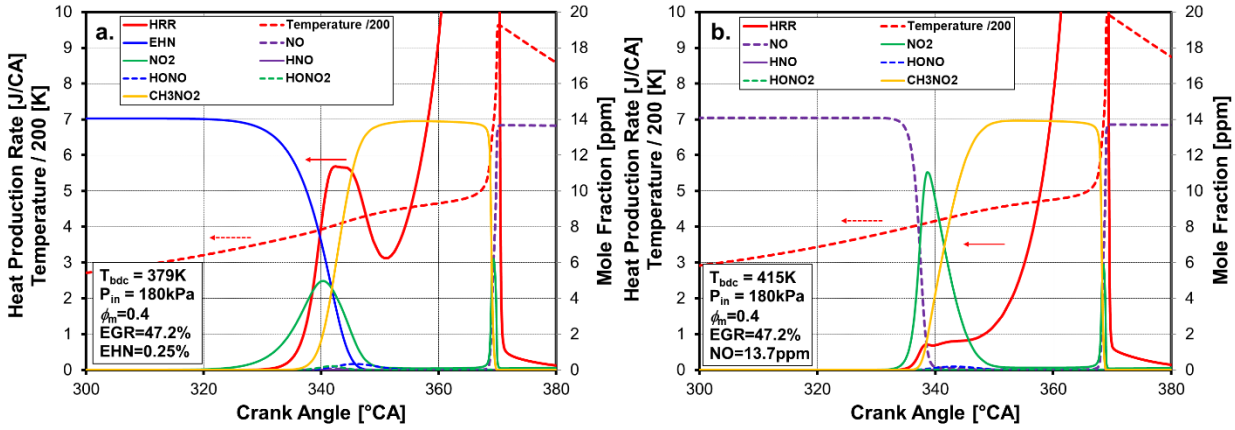

Figure 17. Concentration profiles of several species that contain nitrogen at P_{in} = 180 kPa, ϕ_m = 0.40, EGR = 47.2% for fuel doped with (a) 0.25% EHN, and (b) 13.7 ppm NO.

EHN thermal decomposition occurs approximately 17°CA later than the earlier result with the original sub-mechanism (Fig. 10). The nitrate group of EHN is converted to NO_2 through reaction R1, and this species reacts with the methyl radical (CH_3) to form CH_3NO_2 through the following reaction:

$$CH_3 + NO_2 (+ M) \Leftrightarrow CH_3NO_2 (+ M) \qquad R3$$

This is a third body reaction, with M being any species that absorbs the excess of energy stabilizing the reaction. The maximum NO_2 concentration reached during the EHN decomposition is about 35% of the initial EHN concentration, while it reaches 100% with the original EHN sub-mechanism. This means that the temperature needed for the EHN thermal decomposition with the modified mechanism is high enough to simultaneously activate R3. Nearly all the NO_2

546 produced by R1 is transformed to CH_3NO_2 by R_3. Furthermore, CH_3NO_2 is stable during the ITHR.
547 Therefore, the maximum CH_3NO_2 concentration reaches almost the same value as the initial EHN
548 concentration. CH_3NO_2 dehydrogenation occurs during the high-temperature stage through H-
549 abstraction reactions with presence of several radicals, among which OH is the most relevant.
550 Moreover, CH_3NO_2 dehydrogenation is also a NO production pathway through the following
551 reactions:

552 $$CH_3NO_2 + R' \Leftrightarrow CH_2NO_2 + R\text{-}H \qquad R4$$

553 $$CH_2NO_2 \Leftrightarrow CH_2O + NO \qquad R5$$

554 NO_2 is accumulated again during the high-temperature ignition. However, it is rapidly consumed
555 and transformed to NO via the following reactions:

556 $$NO_2 + OH \Leftrightarrow NO + HO_2 \qquad R6$$

557 $$NO_2 + CH_3 \Leftrightarrow NO + CH_3O \qquad R7$$

558 These reactions appear to be the reason why the kinetic model over-predicts the NO_x emissions,
559 especially the amount of NO, which represents 96.5% of the total amount of NOx. Finally, only
560 traces of HNO, HONO, and $HONO_2$ are found during the autoignition process. This does not mean
561 that the chemistry of these species is negligible, but their production and decomposition rates
562 have the same magnitude and occur almost simultaneously.
563 Fig. 17(b) shows the simulation results with the initial concentration of EHN substituted by NO
564 (13.7 ppm) in order to analyze the chemical pathways followed by this species, since it tends to
565 enhance the ignition. As discussed earlier, NO accelerates the ignition in a lower extent than EHN,
566 so that the required T_{BDC} has to be increased to keep the CA10 constant (from 379 K with EHN
567 to 415 K with NO). Results are very similar to those with EHN. Backward reaction of R6 controls
568 the NO oxidation to NO_2 during the low-temperature stage, which generates OH radicals that
569 accelerate the fuel dehydrogenation and enhance the ignition. After the NO decomposition, the

chemical paths that control the formation and consumption of nitrogenated species are the same as those for EHN-doped fuel. The LTHR and ITHR are less intense when the fuel is doped with NO. A higher temperature is needed to properly phase the ignition, and the absence of additional C_7H_{15}-3 radicals, which are generated via the EHN thermal decomposition, also lead to the less intense heat releases. While NO is an autoignition enhancer, NO_2 consumes CH_3 radicals during the low-to-intermediate temperature stage via reaction R3. The CH_3 consumption reduces the fuel H-abstraction rate, decreasing the reactivity, as it is shown in Fig. 11.

Conclusions

In the present work, the effect of 2-ethylhexyl nitrate (EHN) on the autoignition reactivity of a regular E10 gasoline in an HCCI engine has been studied both experimentally and numerically over a range of intake pressures, intake temperatures and for two doping levels and two EGR rates. A detailed kinetic model that includes EHN and NO/NO_2 sub-mechanisms was used to simulate the autoignition of a newly proposed surrogate fuel, analyzing the differences between base fuel and EHN-doped fuel. The following conclusions can be deducted from the results:

1. The five-components surrogate fuel was validated versus experimental data using an HCCI single zone reactor that includes heat losses to accurately replicate the engine conditions. Slightly higher BDC temperature (5–6 K) is required in the simulations to closely match the experimental combustion phasing. However, the existence of LTHR for the base fuel at equivalence ratio of 0.4, 21.7% EGR and intake pressure of 180 kPa cannot be reproduced by the simulations.
2. The BDC temperature required to properly phase the ignition was reduced by adding EHN. The original kinetic model tends to over-predict the effect of EHN on the autoignition enhancement, which can be corrected by decreasing the reaction rate of the EHN thermal decomposition by a factor of 100. The modified mechanism properly replicates the experimental LTHR and ITHR exhibited with the doped fuel.

3. The EHN decomposition did not notably affect the temperature despite being endothermic, and the autoignition enhancement was mainly achieved by chemical effects. The 3-heptyl radical (C_7H_{15}-3) generated by the EHN decomposition was identified as the main contributor of the autoignition enhancement of the doped fuel. C_7H_{15}-3 production favors the formation of ROOH species that accelerates the OH production in the low temperature region, promoting the low-to-intermediate temperature chemistry.
4. Simulations showed that adding NO_2 slightly reduced the autoignition reactivity, because this species acts as a sink of CH_3 radicals during the low-to-intermediate temperature regime. However, NO increases the reactivity by generating OH radicals through oxidization to NO_2. However, NO enhances the ignition in a lower extent that EHN.
5. NO_x emissions increased when the fuel was doped with EHN. The nitrate group of EHN showed a conversion rate to NOx between 27% and 40% in the experiments. The conversion rate shown in the simulations is equal to 100% due to an inaccurate description of the NO chemistry, which requires a further improvement.

Acknowledgements

The authors would like to thank Tim Gilbertson, Keith Penney, Aaron Czeszynski and Alberto Garcia for their dedicated support of the LTGC Engine Laboratory. Rajavasanth Rajasegar is greatly thanked for providing insightful technical review for this paper.

This work was performed at the Combustion Research Facility, Sandia National Laboratories, Livermore, CA. Support was provided by the U.S. Department of Energy, Office of Vehicle Technologies. Sandia National Laboratories is a multi-mission laboratory managed and operated by National Technology and Engineering Solutions of Sandia, LLC., a wholly owned subsidiary of Honeywell International, Inc., for the U.S. Department of Energy's National Nuclear Security Administration under contract DE-NA0003525. The views expressed in the article do not necessarily represent the views of the U.S. Department of Energy or the United States Government.

Symbols and Abbreviations

AHRR	apparent heat release rate
AKI	anti-knock index
aTDC	after top dead center
BDC	bottom dead center
bTDC	before top dead center
CA	crank angle
CA10	10% burnt point
CA50	50% burnt point
CI	compression-ignition
COV	coefficient of variation
C_p	constant-pressure heat capacity
CR	compression ratio
C_v	constant-volume heat capacity
E10	10%vol ethanol
EGR	exhaust gas recirculation
EHN	2-Ethylhexyl nitrate
EHO	Ethylhexyloxy radical
EVC	exhaust valve closing
EVO	exhaust valve opening
F/C	fuel/charge gas mass ratio
$(F/A)_{stoich}$	stoichiometric fuel/air mass ratio for complete combustion
GDI	gasoline direct injection
HC	unburned hydrocarbons
HCCI	homogeneous charge compression ignition
HRR	heat release rate
$IMEP_g$	gross indicated mean effective pressure
ITHR	Intermediate-temperature heat release
IVC	intake valve closing
IVO	intake valve opening
LHV	lower heating value
LLNL	Lawrence Livermore National Laboratory
LTC	low-temperature combustion
LTGC	low-temperature gasoline compression-ignition
LTHR	low temperature heat release
max	subscript referred to a maximum value
MON	Motor Octane Number
NOx	nitrogen oxides
P	pressure
P_{in}	intake pressure
R	specific gas constant
RCM	rapid compression machine
RI	ringing intensity
RON	Research Octane Number
SI	spark ignition
t	time

T	temperature
T_{BDC}	bottom dead center temperature of the compression stroke
TDC	top dead center
THR	total heat released
T_{in}	intake temperature
γ	adiabatic index (heat capacity ratio)
τ	autoignition time (ignition delay)
ϕ	Air-based equivalence ratio
ϕ_m	Total charge mass-based equivalence ratio

References

[1] J. E. Dec, "Advanced compression-ignition engines—understanding the in-cylinder processes," *Proceedings of the Combustion Institute*, vol. 32, no. 2, pp. 2727–2742, Jan. 2009, 10.1016/j.proci.2008.08.008.

[2] D. Hariharan, M. Rahimi Boldaji, Z. Yan, B. Gainey, and B. Lawler, "Exploring the Effects of Piston Bowl Geometry and Injector Included Angle on Dual-Fuel and Single-Fuel RCCI," *J. Eng. Gas Turbines Power*, vol. 143, no. 11, Nov. 2021, 10.1115/1.4052203.

[3] A. Shah, A. Hoth, C. P. Kolodziej, and T. Rockstroh, "Gasoline fuels properties for multi-mode operation – Observations in a GDI and the CFR engine," *Fuel*, vol. 291, p. 119680, May 2021, 10.1016/j.fuel.2020.119680.

[4] M. Christensen, B. Johansson, P. Amnéus, and F. Mauss, "Supercharged Homogeneous Charge Compression Ignition," presented at the International Congress & Exposition, 1998, p. 980787.

[5] M. Christensen and B. Johansson, "Supercharged Homogeneous Charge Compression Ignition (HCCI) with Exhaust Gas Recirculation and Pilot Fuel," presented at the CEC/SAE Spring Fuels & Lubricants Meeting & Exposition, 2000, pp. 2000-01–1835.

[6] M. Sjöberg and J. E. Dec, "Comparing late-cycle autoignition stability for single- and two-stage ignition fuels in HCCI engines," *Proceedings of the Combustion Institute*, vol. 31, no. 2, pp. 2895–2902, Jan. 2007, 10.1016/j.proci.2006.08.010.

[7] M. Sjöberg and J. E. Dec, "Influence of Fuel Autoignition Reactivity on the High-Load Limits of HCCI Engines," *SAE Int. J. Engines*, vol. 1, no. 1, pp. 39–58, Apr. 2008, 10.4271/2008-01-0054.

[8] M. Sjöberg and J. E. Dec, "Smoothing HCCI Heat-Release Rates Using Partial Fuel Stratification with Two-Stage Ignition Fuels," *SAE Technical Paper 2006-01-0629*, 2006, https://doi.org/10.4271/2006-01-0629.

[9] J. E. Dec, Y. Yang, and N. Dronniou, "Boosted HCCI - Controlling Pressure-Rise Rates for Performance Improvements using Partial Fuel Stratification with Conventional Gasoline," *SAE Int. J. Engines*, vol. 4, no. 1, pp. 1169–1189, 2011, https://doi.org/10.4271/2011-01-0897.

[10] P. Q. E. Clothier, A. Moise, and H. O. Pritchard, "Effect of free-radical release on diesel ignition delay under simulated cold-starting conditions," *Combustion and Flame*, vol. 81, pp. 242–250, 1990.

[11] B. S. Higgins, D. L. Siebers, and A. A. Aradi, "Comparison of 2-ethylhexyl nitrate and fuel composition induced changes in the diesel spray ignition process," *International Journal of Engine Research*, vol. 2, no. 1, pp. 47–67, 2001.

[12] S. D. Schwab, G. H. Guinther, T. J. Henly, and K. T. Miller, "The Effects of 2-Ethylhexyl Nitrate and Di-Tertiary-Butyl Peroxide on the Exhaust Emissions from a Heavy-Duty Diesel Engine," presented at the International Fuels & Lubricants Meeting & Exposition, 1999, pp. 1999-01–1478.

[13] N. Chacko, C. Johnson, P. Varadarajan, S. Sai Srinivas, and T. Jeyaseelan, “A comparative evaluation of cetane enhancing techniques for improving the smoke, NOx and BSFC trade-off in an automotive diesel engine,” *Fuel*, vol. 289, p. 119918, Apr. 2021, 10.1016/j.fuel.2020.119918.
[14] S. Simsek, S. Uslu, H. Simsek, and G. Uslu, “Multi-objective-optimization of process parameters of diesel engine fueled with biodiesel/2-ethylhexyl nitrate by using Taguchi method,” *Energy*, vol. 231, p. 120866, Sep. 2021, 10.1016/j.energy.2021.120866.
[15] Tian Wei, Wang Lenian, Han Zhiqiang, Chu Yunlu, Wang Xiang, and Xia Qi, “Effects of Combustion Parameters on Emissions of Diesel, Diesel/n-Butanol, and Diesel/n-Butanol/2-Ethylhexyl Nitrate Fuels at Different Intake-Oxygen Concentrations in a Diesel Engine,” *Journal of Energy Engineering*, vol. 147, no. 1, p. 04020081, Feb. 2021, 10.1061/(ASCE)EY.1943-7897.0000710.
[16] H. Kumar, A. K. Sarma, and P. Kumar, “Experimental investigation of 2-EHN effects upon CI engine attributes fuelled with used cooking oil-based hybrid microemulsion biofuel,” *Int. J. Environ. Sci. Technol.*, Oct. 2021, 10.1007/s13762-021-03751-y.
[17] G. Labeckas and S. Slavinskas, “Comparative evaluation of the combustion process and emissions of a diesel engine operating on the cetane improver 2-Ethylhexyl nitrate doped rapeseed oil and aviation JP-8 fuel,” *Energy Conversion and Management: X*, vol. 11, p. 100106, Sep. 2021, 10.1016/j.ecmx.2021.100106.
[18] Y. Yang, J. Dec, and N. Dronniou, “Boosted HCCI Combustion Using Low-Octane Gasoline with Fully Premixed and Partially Stratified Charges,” *SAE Int. J. Engines*, vol. 5, no. 3, pp. 1075–1088, 2012, https://doi.org/10.4271/2012-01-1120.
[19] C. Ji, J. Dec, J. Dernotte, and W. Cannella, “Boosted Premixed-LTGC / HCCI Combustion of EHN-doped Gasoline for Engine Speeds Up to 2400 rpm,” *SAE Int. J. Engines*, vol. 9, no. 4, Oct. 2016, doi:10.4271/2016-01-2295.
[20] R. Hanson, S. Kokjohn, D. Splitter, and R. D. Reitz, “Fuel Effects on Reactivity Controlled Compression Ignition (RCCI) Combustion at Low Load,” *SAE Int. J. Engines*, vol. 4, no. 1, pp. 394–411, Apr. 2011, https://doi.org/10.4271/2011-01-0361.
[21] J. Kaddatz, M. Andrie, R. D. Reitz, and S. Kokjohn, “Light-Duty Reactivity Controlled Compression Ignition Combustion Using a Cetane Improver,” *SAE Technical Paper 2012-01-1110*, Apr. 2012, https://doi.org/10.4271/2012-01-1110.
[22] A. B. Dempsey, N. R. Walker, and R. D. Reitz, “Effect of Cetane Improvers on Gasoline, Ethanol, and Methanol Reactivity and the Implications for RCCI Combustion,” *SAE Int. J. Fuels Lubr.*, vol. 6, no. 1, pp. 170–187, Apr. 2013, https://doi.org/10.4271/2013-01-1678.
[23] V. Hosseini, W. S. Neill, H. Guo, W. L. Chippior, C. Fairbridge, and K. Mitchell, “Effects of different cetane number enhancement strategies on HCCI combustion and emissions,” *International Journal of Engine Research*, vol. 12, no. 2, pp. 89–108, 2011, https://doi.org/10.1177/1468087410395873.
[24] C. Ji, J. E. Dec, J. Dernotte, and W. Cannella, “Effect of Ignition Improvers on the Combustion Performance of Regular-Grade E10 Gasoline in an HCCI Engine,” *SAE Int. J. Engines*, vol. 7, no. 2, pp. 790–806, Apr. 2014, https://doi.org/10.4271/2014-01-1282.
[25] A. M. Ickes, S. V. Bohac, and D. N. Assanis, “Effect of 2-Ethylhexyl Nitrate Cetane Improver on NOx Emissions from Premixed Low-Temperature Diesel Combustion,” *Energy Fuels*, vol. 23, no. 10, pp. 4943–4948, Oct. 2009, 10.1021/ef900408e.
[26] S. Tanaka, F. Ayala, and J. C. Keck, “A reduced chemical kinetic model for HCCI combustion of primary reference fuels in a rapid compression machine,” *Combustion and Flame*, vol. 133, pp. 467–481, 2003.
[27] S. S. Goldsborough, M. V. Johnson, C. Banyon, W. J. Pitz, and M. J. McNenly, “Experimental and modeling study of fuel interactions with an alkyl nitrate cetane enhancer, 2-ethyl-hexyl nitrate,” *Proceedings of the Combustion Institute*, vol. 35, no. 1, Jul. 2014, 10.1016/j.proci.2014.06.048.

[28] M. Hartmann *et al.*, “Experiments and modeling of ignition delay times, flame structure and intermediate species of EHN-doped stoichiometric n-heptane/air combustion,” *Proceedings of the Combustion Institute*, vol. 32, no. 1, pp. 197–204, Jan. 2009, 10.1016/j.proci.2008.06.068.
[29] C. A. Almodovar and C. F. Goldsmith, “Laser schlieren study of the thermal decomposition of 2-ethylhexyl-nitrate,” *Proceedings of the Combustion Institute*, vol. 38, no. 1, pp. 997–1005, Jan. 2021, 10.1016/j.proci.2020.07.105.
[30] Y. Stein, R. A. Yetter, F. L. Dryer, and A. Aradi, “The Autoignition Behavior of Surrogate Diesel Fuel Mixtures and the Chemical Effects of 2-Ethylhexyl Nitrate (2-EHN) Cetane Improver,” presented at the International Fuels & Lubricants Meeting & Exposition, 1999, pp. 1999-01–1504.
[31] P. U. Ricklin, A. Kazakov, F. L. Dryer, S. C. Kong, and R. D. Reitz, “The Effects of NOx Addition on the Auto Ignition Behavior of Natural Gas under HCCI Conditions,” presented at the Spring Fuels & Lubricants Meeting & Exhibition, 2002, pp. 2002-01–1746.
[32] P. Risberg, D. Johansson, J. Andrae, G. Kalghatgi, P. Björnbom, and H.-E. Ångström, “The Influence of NO on the Combustion Phasing in an HCCI Engine,” *SAE Technical Paper 2006-01-0416*, Apr. 2006, 10.4271/2006-01-0416.
[33] D. Lopez Pintor, J. E. Dec, and G. Gentz, “Experimental evaluation of a custom gasoline-like blend designed to simultaneously improve ϕ-sensitivity, RON and octane sensitivity,” *SAE Int. J. Adv. & Curr. Prac. in Mobility*, vol. 2, no. 4, pp. 2196–2216, 2020, https://doi.org/10.4271/2020-01-1136.
[34] D. Lopez Pintor, G. Gentz, and J. Dec, “Mixture Stratification for CA50 Control of LTGC Engines with Reactivity-Enhanced and Non-Additized Gasoline,” *SAE Technical Paper 2021-01-0513*, Apr. 2021, 10.4271/2021-01-0513.
[35] G. Gentz, J. Dernotte, C. Ji, D. Lopez Pintor, and J. Dec, “Combustion-Timing Control of Low-Temperature Gasoline Combustion (LTGC) Engines by Using Double Direct-Injections to Control Kinetic Rates,” *SAE Technical Paper 2019-01-1156*, Apr. 2019, https://doi.org/10.4271/2019-01-1156.
[36] H. O. Pritchard, “Thermal decomposition of isooctyl nitrate,” *Combustion and Flame*, vol. 75, no. 3, pp. 415–416, Mar. 1989, 10.1016/0010-2180(89)90052-7.
[37] Y. Yamaya, M. Furutani, and Y. Ohta, “Premixed Compression Ignition of Formaldehyde-Doped Lean Butane/Air Mixtures in a Wide Range of Temperature,” *SAE Technical Paper 2004-01-1977*, Jun. 2004, 10.4271/2004-01-1977.
[38] Y. Yang, J. E. Dec, N. Dronniou, and M. Sjöberg, “Tailoring HCCI heat release rates with partial fuel stratification: comparison of two-stage and single-stage ignition fuels,” *Proceedings of the Combustion Institute*, vol. 33, pp. 3047–3055, 2011, https://doi.org/10.1016/j.proci.2010.06.114.
[39] J. B. Heywood, *Internal combustion engine fundamentals*. New York: McGraw-Hill, 1988.
[40] G. Woschni, “A Universally Applicable Equation for the Instantaneous Heat Transfer Coefficient in the Internal Combustion Engine,” *SAE Paper no. 670931*, 1967, https://doi.org/10.4271/670931.
[41] D. Lopez-Pintor and J. E. Dec, “Experimental Evaluation of a Gasoline-like Fuel Blend with High Renewable Content to Simultaneously Increase ϕ-Sensitivity, RON, and Octane Sensitivity,” *Energy Fuels*, vol. 35, no. 20, pp. 16482–16493, Oct. 2021, 10.1021/acs.energyfuels.1c01979.
[42] K. Lee, S. Cho, N. Kim, and K. Min, “A study on combustion control and operating range expansion of gasoline HCCI,” *Energy*, vol. 91, pp. 1038–1048, 2015, https://doi.org/10.1016/j.energy.2015.08.031.
[43] M. Mehl, W. J. Pitz, C. K. Westbrook, and H. J. Curran, “Kinetic modeling of gasoline surrogate components and mixtures under engine conditions,” *Proceedings of the Combustion Institute*, vol. 33, pp. 193–200, 2011.
[44] M. Sjoberg and J. E. Dec, “Ethanol Autoignition Characteristics and HCCI Performance for Wide Ranges of Engine Speed, Load and Boost,” *SAE Int. J. Engines*, vol. 3, no. 1, pp. 84–106, Apr. 2010, 10.4271/2010-01-0338.

[45] H. Bornemann, F. Scheidt, and W. Sander, “Thermal decomposition of 2-ethylhexyl nitrate (2-EHN),” *International Journal of Chemical Kinetics*, vol. 34, no. 1, pp. 34–38, 2002, https://doi.org/10.1002/kin.10017.
[46] C. L. Rasmussen, A. E. Rasmussen, and P. Glarborg, “Sensitizing effects of NOx on CH4 oxidation at high pressure,” *Combustion and Flame*, vol. 154, no. 3, pp. 529–545, Aug. 2008, 10.1016/j.combustflame.2008.01.012.
[47] M. Sjöberg and J. E. Dec, “An Investigation of the Relationship Between Measured Intake Temperature, BDC Temperature, and Combustion Phasing for Premixed and DI HCCI Engines,” presented at the 2004 SAE Fuels & Lubricants Meeting & Exhibition, 2004, pp. 2004-01–1900.
[48] J. E. Dec, Y. Yang, and N. Dronniou, “Improving Efficiency and Using E10 for Higher Loads in Boosted HCCI Engines,” *SAE International Journal of Engines*, vol. 5, no. 3, pp. 1009–1032, Apr. 2012, 10.4271/2012-01-1107.
[49] J. E. Dec and Y. Yang, “Boosted HCCI for High Power without Engine Knock and with Ultra-Low NOx Emissions - using Conventional Gasoline,” *SAE Int. J. Engines*, vol. 3, no. 1, pp. 750–767, 2010, https://doi.org/10.4271/2010-01-1086.